Skeleton-Based Bilateral Symmetry: Theoretical Concepts and Detection via Dynamic Programming

Nikita Lomov[a], Oleg Seredin[b] and Olesia Kushnir[c]
Tula State University, Prospekt Lenina, 92, Tula, 300012, Russia

Keywords: Skeleton, Bilateral Symmetry, Medial Representation, Jaccard Index, Dynamic Programming.

Abstract: This study presents a formal definition and an algorithm for the detection of bilateral symmetry in flexible planar objects. We proposed to analyze the skeleton of a 2D figure and detect its symmetry using the automorphism of the original and reflected skeleton graphs enhanced with additional requirements. The axis of symmetry is formed by the skeleton edges invariant under reflection. We developed a dynamic programming algorithm that finds the optimal mapping of the half-edges of the skeleton considering their "duality". We also implemented a symmetrization of the skeleton and original figure, making the detected axis the figure's vertical axis of reflective symmetry. We showed that the optimized target value when searching for the skeletal mapping agrees well with the Jaccard similarity index.

1 INTRODUCTION

Symmetry is an important feature of many objects perceived by human vision. Symmetry detection tools are important for many computer graphics and computer vision applications such as morphing, object classification, style transfer, parametrization, etc. Apart from the intuitive concept of symmetry as "something composed of identical elements" or "self-similar", symmetry is a meaningful mathematical concept. It implies the existence of a transformation that does not change the object's shape when its parts are rearranged. The simplest examples are reflection and rotation. The points invariant to such transformations (the axis of reflection and the center of rotation) are called the center of the object.

Symmetry detection is complicated for real-world objects captured by cameras, scanners, and sensors. First, the transformation becomes rather complex. Second, even when the formal transformation applies, complete self-similarity of the object is impossible. The first aspect is mostly attributed to the fact that real-world shapes are at least partly flexible, so the axis of symmetry is curvilinear; besides, segments of many living beings can articulate independently of the major axis. Human arms are a good example of this. As a result, the definition of symmetry through only one axis is insufficient. We need to specify how the pairs of the object points map onto each other.

The symmetry of a planar figure requires a pairwise correspondence between all the points of the figure. Any planar shape can be represented by a set of lines with non-zero thickness and is completely "packed" into a skeleton, a set of its skeleton axes. The skeleton of a 2D figure is a planar graph, so we can apply the well-developed graph theory to the symmetry analysis.

The purpose of this study is to rigorously formalize the concept of planar graph symmetry and develop a symmetry detection algorithm. The proposed algorithm can be applied to the analysis of planar figures defined as their medial representations to evaluate the degree of symmetry and symmetrization. Our experiments show that the proposed symmetry index correlates well with the Jaccard index of the figure after symmetrization. The algorithm is versatile and offers high computational efficiency.

2 RELATED WORK

The simplest type of bilateral symmetry that requires a nontrivial deformation of the figure is curvilinear symmetry. It is completely defined by the equation of its axis. A method for detecting all possible curvilinear axes approximated by polylines using a dynamic programming algorithm is proposed in (Lomov

[a] https://orcid.org/0000-0003-4286-1768
[b] https://orcid.org/0000-0003-0410-7705
[c] https://orcid.org/0000-0001-7879-9463

Lomov, N., Seredin, O. and Kushnir, O.
Skeleton-Based Bilateral Symmetry: Theoretical Concepts and Detection via Dynamic Programming.
DOI: 10.5220/0013321400003912

In *Proceedings of the 20th International Joint Conference on Computer Vision, Imaging and Computer Graphics Theory and Applications (VISIGRAPP 2025) - Volume 3: VISAPP*, pages 746-754
ISBN: 978-989-758-728-3; ISSN: 2184-4321

and Seredin, 2023). A greedy algorithm for tracing a curvilinear symmetry axis is proposed in (Seredin et al., 2023). It aims to pass the points with the best local symmetry along the normal to the path. A graph-based algorithm is used in (Liu and Liu, 2011) to construct the symmetry axis as a polyline for the full-color image region so that the characteristic of the polyline at each point is the spread (the length of the symmetric perpendicular section).

In (Huang et al., 2023), a planar shape is represented by a polygon for which an integer programming algorithm finds the optimal mapping of the sides.

An approach that reduces the symmetry detection problem to mapping chains of skeleton primitives is discussed in (Kushnir et al., 2017). The properties of skeleton edges are length, angle of rotation relative to the previous edge (in the order of traversal), and the width of the figure along the edge. For the efficiency of comparison, the width is defined by the Legendre polynomial's coefficients.

In (Qian et al., 2015), the authors consider the main chain of the skeleton as the axis of curvilinear symmetry and introduce a mutual correspondence between the terminal vertices of the skeleton and the chains connecting these vertices. The properties of the vertices are the distances to the axis, the proximity of their joint points, and the width of the figure in the vicinity of the point. The edges are defined by the ratio of geodesic distances between their ends. A genetic algorithm is used to find the optimal mapping. For symmetrization, the shape width between the corresponding branches of the skeletal graph is averaged.

The method proposed in (Yang et al., 2008) divides the contour into two parts. They are compared using the distribution of geodesic distances between their critical points measured along the contour. A similar approach is used in (Bai and Latecki, 2008) to compare two different shapes for image classification. The distances are measured along the skeleton edges.

Note that the methods analyzing the distribution of skeletal distances can be generalized to 3D shapes and therefore are quite popular. In (Wang et al., 2019), skeletons are used to map convex shape fragments that have extrinsic symmetry, ultimately defining intrinsic symmetry. Another area of research is the analysis of 3D skeletons represented by point clouds (Jiang et al., 2013) or triangular meshes (Nagar and Raman, 2018). Reflective symmetry of rigid 3D shapes is studied in (Cicconet et al., 2017) in terms of the point cloud mapping problem. Methods for direct analysis of 3D skeletons with various representations are developed in (Song et al., 2018; Huang et al., 2013).

Self-symmetry of the shape can be an issue because the dual points have similar properties. This drawback is analyzed in (Xu and Zhang, 2016) as applied to human 3D skeletons. The symmetry of many organic shapes is analyzed in (Li et al., 2019) to map the parts of two symmetrical shapes (such as animal figures). For this, an axis of symmetry is detected in each skeleton by comparing subgraphs connected to the axis candidate, and subgraphs of the different shapes with similar intrinsic properties are compared. A correspondence between two symmetric 3D shapes is sought in (Liu et al., 2012), but the symmetry is defined by a closed curve on the surface.

However, the proposed methods do not allow one to directly derive a normalized and well-interpretable measure of symmetry for 2D shapes.

3 PLANE SHAPE SKELETONS

It is reasonable to digitally represent the shape of objects as binary raster images. However, we consider continuous skeletonization resulting in planar shapes and skeletons represented as parametric curves, since this is much more convenient for analytical processing.

A figure is a closed region bounded by a finite number of non-intersecting Jordan curves. The skeleton S of a figure A is the closure of the set of shape points having several nearest boundary points. The radial function $r(c) : S \to \mathbb{R}_+$ takes the value of the radius of the largest circle centered at s and inscribed in the shape. We will denote the circle as $B(c)$. The skeleton and radial function combined are called the medial representation. We will also define a silhouette $H(S')$ for the skeleton's fragment $S' \subseteq S$: $H(S') = \cup_{c \in S'} B(c)$. Since $A = H(S)$, a conversion to the medial representation allows us to completely reconstruct the original shape and preserves all the shape information.

The medial representation exists for all planar shapes, but for real-life applications, it is convenient to restrict the range of shapes to polygonal shapes whose boundaries are simple polygons. In this case, the skeleton consists of a finite number of straight and parabolic segments, while the radial function has a simple analytic form. Any shape can be approximated by a polygon with sufficient accuracy. Since the skeletons may have many occasional edges, a pruning procedure is used to simplify the skeleton by removing the edges that have little effect on the silhouette. The basic concepts of skeletons are shown in Fig. 1.

To approximate the shape of binary image objects

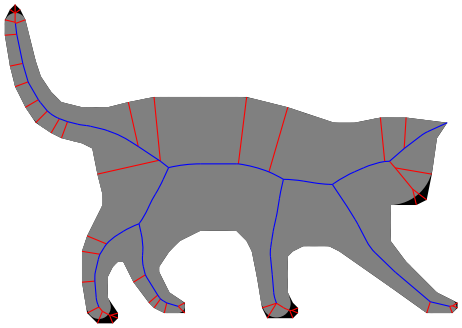

Figure 1: Skeleton of a planar shape approximated by a polygon. Red: branches removed by pruning. Blue: remaining branches. Grey: their silhouette. Black: part of the shape lost due to pruning.

with polygonal figures and calculate their skeletons, we used the algorithms described in (Mestetskiy and Semenov, 2008; Mestetskiy and Koptelov, 2024). It is reasonable to consider that for a shape with some symmetry its skeleton graph is also symmetric. The formalization of planar graph bilateral symmetry will be discussed below.

4 DEFINITION OF SKELETAL SYMMETRY

Let us consider an undirected planar graph $G = (V,E)$. It has reflective symmetry, if there exists a rectilinear planar embedding $g : V \to \mathbb{R}^2$, $g(u) = (x(u),y(u))$, which is symmetric about Y-axis:

$$\forall (u,u') \in E \; \exists (v,v') \in E :$$
$$g(v) = (-x(u),y(u)),\; g(v') = (-x(u'),y(u')).$$

We will consider the vertices for which $x(u) < 0$ to be left ones and belonging to the set $\mathcal{L}$. The set of right vertices $\mathcal{R}$ contains the vertices for which $x(u) > 0$. Finally, the vertices with $x(u) = 0$ constitute the set of center vertices $\mathcal{C}$. Then we can define the symmetry in terms of the graph itself: there exists an automorphism $f : V \to V$ such that:

1. $f(u) = v \implies f(v) = u$,
2. $u \in \mathcal{L} \implies f(u) \in \mathcal{R}$,
3. $(u,v) \in E$ and $u \in \mathcal{L}$ and $v \in \mathcal{R} \implies f(u) = v$,
4. We cannot move any elements from $\mathcal{C}$ to $\mathcal{L}$ and $\mathcal{R}$ keeping the above properties intact.

Note that the contrary is also true: if such an automorphism exists, then the corresponding planar embedding also exists.

Examples of symmetric and asymmetric graphs are shown in Fig. 2. Note that the symmetrizing automorphism f can be defined in multiple ways and specify various axes of symmetry.

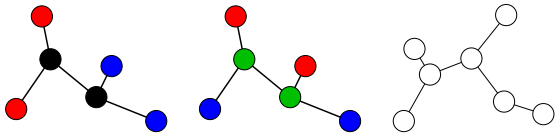

(a) (b) (c)

Figure 2: Symmetric (a,b) and non-symmetric (c) graphs. Pairs of vertices with the same color are symmetric to each other. Black vertices map into themselves.

5 SEARCH FOR OPTIMAL SKELETAL SELF-MATCHING

Let us construct a connected, undirected, acyclic planar graph $G = (V,E)$ with half-edges $\hat{E} = \bigcup_{(u,v)\in E}\{u \to v, v \to u\}$. Using a planar embedding of graph G, for each vertex u and its incident vertex v, we can create a function $\text{next}_v(u) : V \to V$, which defines the final vertex of the edge $v \to u'$ following counterclockwise the edge $v \to u$. Then, starting from an arbitrary half-edge $e \in \hat{E}$, we can find a unique order of traversal for the graph G (Algorithm 1). As a result, the list T will contain all $2|E|$ half-edges of G without repetitions.

Data: Graph $\hat{G} = (V,\hat{E})$, embedding g
Result: Traversal T
Choose any $e \in \hat{E}$;
$T = []$;
$e_0 = e$;
do
  T.append(e);
  $e = v \to \text{next}_{v(e)}(u(e))$;
while $e \neq e_0$;

Algorithm 1: Planar graph traversal.

Let us symmetrically reflect the embedding of the graph G. Then during its traversal, the next clockwise edge will be *previous* in the original embedding. Therefore, a new traversal T' can be obtained by arranging the edges in T in reverse order.

Let $T = [t_1,t_2,\ldots t_n]$, $T' = [t'_1,t'_2,\ldots t'_n]$, and a function p defines the index of the twin half-edge: $t_i = u \to u'$, $t_j = u' \to u \implies p(i) = j$. The function $p'(i)$ is defined similarly. For a symmetric graph G, we construct a one-to-one correspondence s between the elements of T and T': for $f(u) = v$, $f(u') = v'$, $t_i = u \to u'$, $t'_j = v \to v'$, $s(i) = j$. The opposite is also true: we can restore the automorphism f from that

Data: Traversals T, T', $|T| = n$, $|T'| = m$
Function *align*(i_1, i_2, j_1, j_2)
  if $R(i_1, i_2, j_1, j_2) \geq 0$ **then**
    ; // do nothing
  end
  else if $j_1 > j_2$ **then**
    $r = 0$; // $\widetilde{T}'$ is empty
    for $i = i_2, \ldots, i_1$ **do**
      $r = r + w_{i0}$;
      $R(i, i_2, j_1, j_2) = r$;
      $B(i, i_2, j_1, j_2) = 1$;
    end
  end
  else if $i_1 > i_2$ **then**
    $r = 0$; // $\widetilde{T}$ is empty
    for $j = j_2, \ldots, j_1$ **do**
      $r = r + w_{0j}$;
      $R(i_1, i_2, j, j_2) = r$;
      $B(i_1, i_2, j, j_2) = 2$;
    end
  end
  else
    $d = [w_{i0} + \text{align}(i_1 + 1, i_2, j_1, j_2),$
    $w_{0j} + \text{align}(i_1, i_2, j_1 + 1, j_2)]$;
    if $p(i_1) > i_1$ **then**
      d.append$(2w_{i_1 j_1} + \text{align}(i_1 +$
       $1, p(i_1) - 1, j_1 + 1, p'(j_1) - 1) +$
       $\text{align}(p(i_1) + 1, i_2, p'(j_1) + 1, j_2)$;
    end
    $R(i_1, i_2, j_1, j_2) = \min d$;
    $B(i_1, i_2, j_1, j_2) = \arg\min d$;
  end
  return $R(i_1, i_2, j_1, j_2)$;
end

Algorithm 2: Calculation of the symmetry functional as the similarity of skeleton subsequences.

one-to-one correspondence. It is also obvious that $s(p(i)) = p'(s(i))$.

If the graph is not symmetric, it can be made symmetric by a sequence of edge contractions. In the extreme case, we get a graph with just one vertex, which is symmetric by definition. Note that when contracting the edge (u, u'), in the traversal sequence T both half-edges $u \to u'$ and $u' \to u$ are simply eliminated, and the vertices u and u' are replaced by the merged vertex u''. Therefore, the minimum number of edge removals from T and T', allowing to establish a bijection between T and T', determines the minimum number of edge contractions that make G symmetric. We can assume that for a half-edge t_i to be removed $s(i) = \varepsilon$, so at the smallest number of contractions, the number of such t_i is the smallest.

Result: s function values:
  $S = [s(1), s(2), \ldots, s(n)]$
Procedure *backtrace*(i_1, i_2, j_1, j_2)
  if $i_1 > i_2$ *or* $j_1 > j_2$ **then**
    return;
  end
  if $B(i_1, i_2, j_1, j_2) = 1$ **then**
    // skip in T
    backtrace$(i_1 + 1, i_2, j_1, j_2)$;
  end
  if $B(i_1, i_2, j_1, j_2) = 2$ **then**
    // skip in T'
    backtrace$(i_1, i_2, j_1 + 1, j_2)$;
  end
  else
    $s(i_1) = j_1$;
    $s(p(i_1)) = p'(j_1)$;
    backtrace$(i_1 + 1, p(i_1) - 1, j_1 +$
     $1, p'(j_1) - 1)$;
    backtrace$(p(i_1) + 1, i_2, p''(j_1) + 1, j_2)$;
  end
end
$s(i) \leftarrow \varepsilon$, $i = 1, \ldots n$;
$R \leftarrow -\text{ones}(n, n, m, m)$; // Rewards
$B \leftarrow \text{zeros}(n, n, m, m)$; // Steps
align$(1, n, 1, m)$;
backtrace$(1, n, 1, m)$;

Algorithm 3: Restoration of optimal matching.

Note that in the case of a symmetric G, there exists T'', a cyclic shift of T', such that $s(i) = i$, $i = 1, \ldots, n$ (here s links T and T''). Therefore, for a non-symmetric G there exists a shift T'' for which

$$s(i_1) \neq \varepsilon \text{ and } s(i_2) \neq \varepsilon \text{ and } i_1 < i_2 \implies s(i_1) < s(i_2).$$

The optimal solution of the problem with mapped t_i and $t'_{s(i)}$ includes the optimal matching of subsequences $\widetilde{T} = [t_{i+1}, t_{i+2}, \ldots t_{p(i)-1}]$ and $\widetilde{T}' = [t'_{s(i)+1}, t'_{s(i)+2}, \ldots t'_{p'(s(i))-1}]$. It allows us to use the dynamic programming approach (Algorithm 2), where the difference between is $\widetilde{T}$ and $\widetilde{T}'$ is stored in $R(i + 1, p(i) - 1, s(i) + 1, p'(s(i)) - 1)$.

Algorithm 2 must be applied to all cyclic shifts of T'. In this case, the results can be reused. It is sufficient to assume that the indices j_1 and j_2 are also shifted by some k and to perform checks for $j_1 - k$ and $j_2 - k$ modulo m. Besides, if T' is a traversal of the graph T in reverse order, then due to the data duplication $R(i_1, i_2, j_1, j_2) = R(n + 1 - j_2, n + 1 - j_1, n + 1 - i_2, n + 1 - i_1)$, $B(i, p(i), j, p(j)) = 3 \implies B(n + 1 - p(j), n + 1 - j, n + 1 - p(i), n + 1 - i) = 3$.

The weights w_{i0}, w_{0j}, and w_{ij} are penalties for missing i-th element in T, j-th element in T', and

for mapping such elements, respectively (the penalty does not change when both edges are reversed so that $w_{ij} = w_{p(i)p'(j)}$).

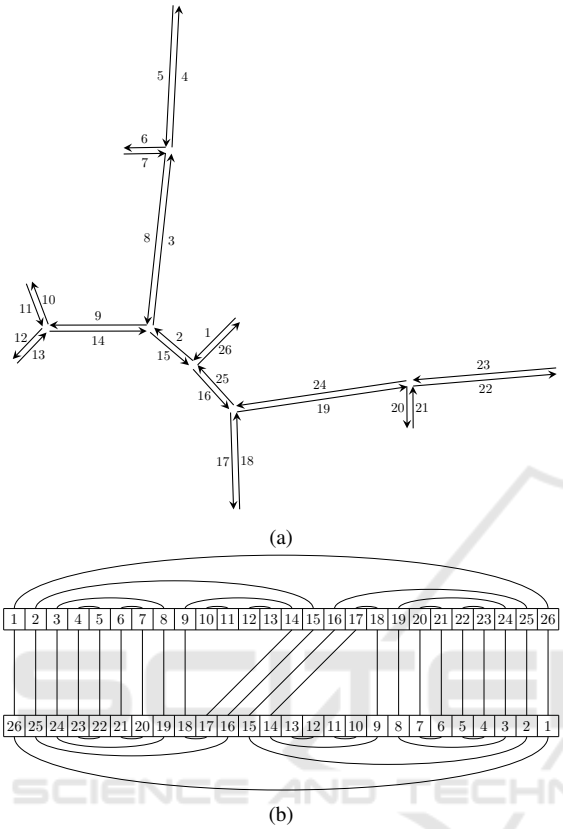

Figure 3: (a) Graph traversal, and (b) edge mapping for the subgraph with maximum symmetry. The twin half-edges are connected by arcs.

An example of optimal graph matching with its reflection, restored by Algorithm 3, is shown in Fig. 3. Note that edges have not yet been assigned any properties, the penalties for missing edges are 1, and the penalties for matching edges are 0.

6 CHARACTERIZATION OF EDGES

To analyze the degree of symmetry of the shape A, area-based metrics are commonly used. One of them is the Jaccard index $J(A,A') = \frac{|A \cap A'|}{|A \cup A'|}$, where A' is the transformation (e.g. reflection) of the shape A. When searching for the symmetry parameters, we aim to maximize this value. The Jaccard index can be defined from the dissimilarity of the figures:

$$J(A,A') = \frac{|A \cap A'|}{|A \cap A'| + |A \triangle A'|} = \frac{|A| + |A'| - |A \triangle A'|}{|A| + |A'| + |A \triangle A'|},$$

since $2|A \cap A'| + |A \triangle A'| = |A| + |A'|$. Maximizing the Jaccard index is equivalent to minimizing the dissimilarity $|A \triangle A'|$. For the graph shown in Fig. 3a we can consider that $|T| = |T'| = 26$, $|T \setminus T'| = |T' \setminus T| = 4$, and $|T \triangle T'| = 8$. Therefore, the potential Jaccard index is $\frac{44}{60} = 0.733$.

Since dynamic programming requires problem decomposition, it is reasonable to assume that the entire area of the shape is distributed along individual edges. Let the skeleton S of the shape A contains the edges $\{e_i\}_{i=1}^k$, where $e_i = (x_i(t), y_i(t))$, $t \in [0,1]$, $i = 1, \ldots, k$. Let us define the density $q(c) \in \mathbb{R}_+$ at each point $c \in S$ in such a way that $\sum_{i=1}^k a_i = |A|$, where

$$a_i = \int_0^1 q(x_i(t), y_i(t)) \sqrt{(x_i'(t))^2 + (y_i'(t))^2} dt.$$

This equality is preserved for any partitioning into edges.

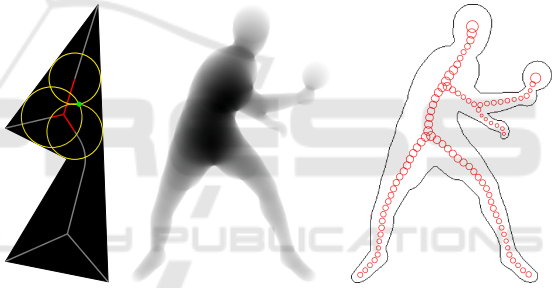

(a) (b) (c)

Figure 4: (a) Part of the skeleton (highlighted in red) with circles covering a given point. (b) Visualization of the $l(p)$ function. (c) Visualization of the $q(c)$ function, circle areas are proportional to function values.

To choose $q(c)$, we use the criterion of point c "importance" for the construction of shape A. It is the higher, the less other points of the skeleton can recover the points of circle $B(c)$. Let $S'(p) = \{c \in S : p \in B(c)\}$ for point $p \in A$, and $l(p) = |S'(p)|$ (the total length of curves in $S'(p)$). Then

$$q(c) = \iint_{p \in B(c)} \frac{1}{l(p)} dp.$$

It means that all points of A are distributed equally over all centers of the circles covering them. Fig. 4 shows an example of determining the values of $l(p)$ and $q(c)$.

We use $\{a_i\}$ as weights (penalties) for missing edges: $w_{i0} = a_i$, $w_{0j} = a_{n+1-i}$. We set the mapping penalties as $w_{ij} = |a_{n+1-j} - a_i|$ (recall that j-th edge in T' is $(n+1-j)$-th in T). For better accuracy of

the area dissimilarity estimations, it is reasonable to make the edges $\{e_j\}$ both sufficiently short and approximately equal. To do this, we find the maximum length of the edge $l_{\max}$ and break the skeleton branch (path between terminals and forks) of length l into $\lceil \frac{l}{l_{\max}} \rceil$ edges of equal length. Since the original skeleton edges are straight or parabolic segments, their lengths can be calculated analytically. An example of such a skeleton's unification is shown in Fig. 5. As a result, the skeleton has 46 edges instead of 117.

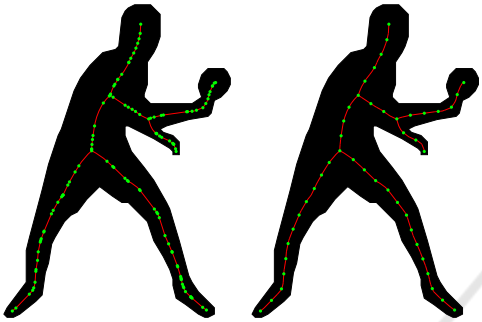

(a) (b)

Figure 5: (a) Vertices of the original skeleton. (b) Vertices of the unified skeleton.

Since Algorithm 2 has to calculate the values of $R(i_1,i_2,j_1,j_2)$ for all possible values of the four indices, the total complexity of the exact algorithm is $O(|E|^4)$. To improve the performance, we can apply the algorithm at the level of skeleton branches. Let the branch b_i consist of edges with areas $\mathbf{a}_i = [a_{i1},\ldots,a_{in'}]$, and the branch b_j consists of edges with areas $\mathbf{a}_j = [a_{j1},\ldots,a_{jn''}]$. Then $w_i = \sum_{t=1}^{n'} a_{it}$, and $w_{i,n+1-j}$ is found through optimal mapping of $\mathbf{a}_i$ and $\mathbf{a}_j$ by the dynamic time warping (DTW) algorithm with the same penalties as for the individual edges. Since the DTW complexity of a pair of branches is $O(n'n'')$, and we need to compare each branch to each branch, the total complexity is $O(|E|^2)$.

7 IMAGE STRAIGHTENING

Shape straightening means making the shape reflectively symmetric. For this, the skeleton axis of symmetry is turned vertical, and the reflected skeleton edges are placed at equal angles to the axis. Unlike the symmetrization procedure described in (Qian et al., 2015), we do not average the widths of the skeleton edges but average the angles. Therefore these procedures complement each other. The straightening only rotates the skeleton edge, which can be considered a flexible transformation of the planar shape.

Let E' be the set of the skeleton edges, forming an axis of symmetry, i.e. invariant to the mapping, $V' = \{v'_1,\ldots,v'_l\}$ is the set of their vertices in the chain traversal order. To make the edge $e'_i = (v'_i, v'_{i+1})$ vertical, it must be rotated by the angle $\gamma_i = \frac{\pi}{2} - \operatorname{atan2}(y(v'_{i+1}) - y(v'_i), x(v'_{i+1}) - x(v'_i))$.

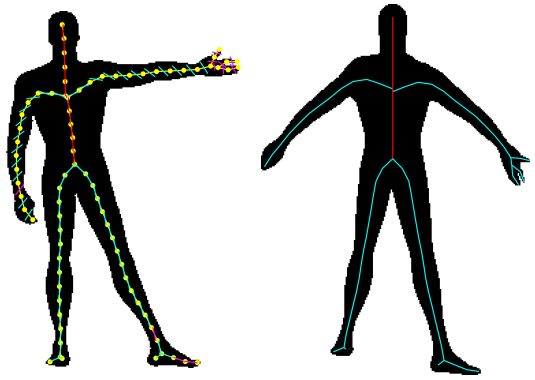

Figure 6: Standardization of the shape articulation. (a) Original shape with subdivided edges. New directions of the edges after straightening: red: axial; blue: having a pair; pink: unmapped. (b) Straightened shape and its skeleton.

Each mapped pair of edges (u_1,v_1) and (u_2,v_2) with angles α_1 and α_2 between vertices is rotated by the angle $\gamma_j + \beta$ with the minimum absolute value β such as:

$$\frac{\alpha_1+\alpha_2}{2} + \gamma_j + \beta \in \left\{+\frac{\pi}{2}, -\frac{\pi}{2}\right\},$$

where γ_j is determined from the edge in E' nearest to the pair.

For an unmapped edge, we find the rotation angle by averaging the angles of the nearest mapped edges in the skeleton graph. When the rotation angles are available, we sequentially recalculate the coordinates of the vertices by descending the skeleton tree. The root is v'_1. The final shape is constructed by drawing the edge silhouettes with the same radii of the circles but in new positions.

Fig. 6 shows the result of straightening. The straightened shape can be used to estimate the final degree of symmetry with the Jaccard index, taking the $x = x(v'_1)$ line as the symmetry axis. In this case, the Jaccard index J is 0.833, and its approximation by the mapping algorithm $\tilde{J} = \frac{4|A|-R(1,n,1,n)}{4|A|+R(1,n,1,n)}$ is 0.824.

8 EXPERIMENTS

We tested the proposed methods with 11 images of complex shapes with non-rigid symmetry presented

in (Qian et al., 2015). The length of the edge $l_{\max}$ is $0.03\sqrt{WH}$, where W and H are the width and height of the image. The pruning threshold which defines the maximum Hausdorff distance to the original silhouette is 1 pixel. We used the accelerated version of the method: it compares branches rather than skeleton edges. We also tested the alternative method for finding the curvilinear axis described in (Seredin et al., 2023).

Fig. 7 shows that the proposed method finds the symmetry axis which is either similar to or better than provided by the alternative method. An advantage of the proposed method is the highly efficient image straightening procedure which can straighten fragments of the share separately from the symmetry axis. The results are better both aesthetically and in terms of the Jaccard index: in most cases, it is higher for straightened images. Note that the correlation of the Jaccard index J and its approximation $\tilde{J}$ for this set is 0.8165.

Let us discuss the reasons for the method failure with these images. Fig. 8ab shows the effects of the area characteristics of the skeleton edges. In terms of the Jaccard index, it is more favorable to compare the shape fragments that are close in size (top row) rather than semantically identical (middle row). If we ignore the area and consider all branches of the skeleton as individual edges, the skeleton would be symmetric in the strict sense of graph symmetry, but the symmetry axis again deviates from the desired one (bottom row). The example shows that even for simple shapes, the perception of symmetry is not purely geometric, but involves external information.

The importance of proper selection of the pruning parameter is shown in Fig. 8cd. In the upper row, the ears cannot be mapped completely because the left ear consists of several branches due to the noise (an extra skeleton branch). The problem is solved by increasing the acceptable threshold ρ of the Hausdorff distance between the silhouettes of the original and clipped skeletons from 3 to 4 pixels (middle row). An alternative solution to the problem is using the exact edge-level method. Then not only entire branches, but their parts can be compared. A disadvantage of this approach is the dramatic increase in the number of edges, and decrease in performance. For this example, the number of edges increases from 25 to 104, and the runtime, from 8 milliseconds to 4 seconds, i.e., by a factor of 500.

To evaluate the performance with obviously symmetric shapes, we used 95 images of butterflies from the animal dataset (Bai et al., 2009) (total number of images is 100, but 5 butterflies are shown with their wings folded and have no symmetry). For $\rho = 4$, $l_{\max} = 0.05\sqrt{WH}$, the symmetry axis is correctly found in 71 images when processing branches, and

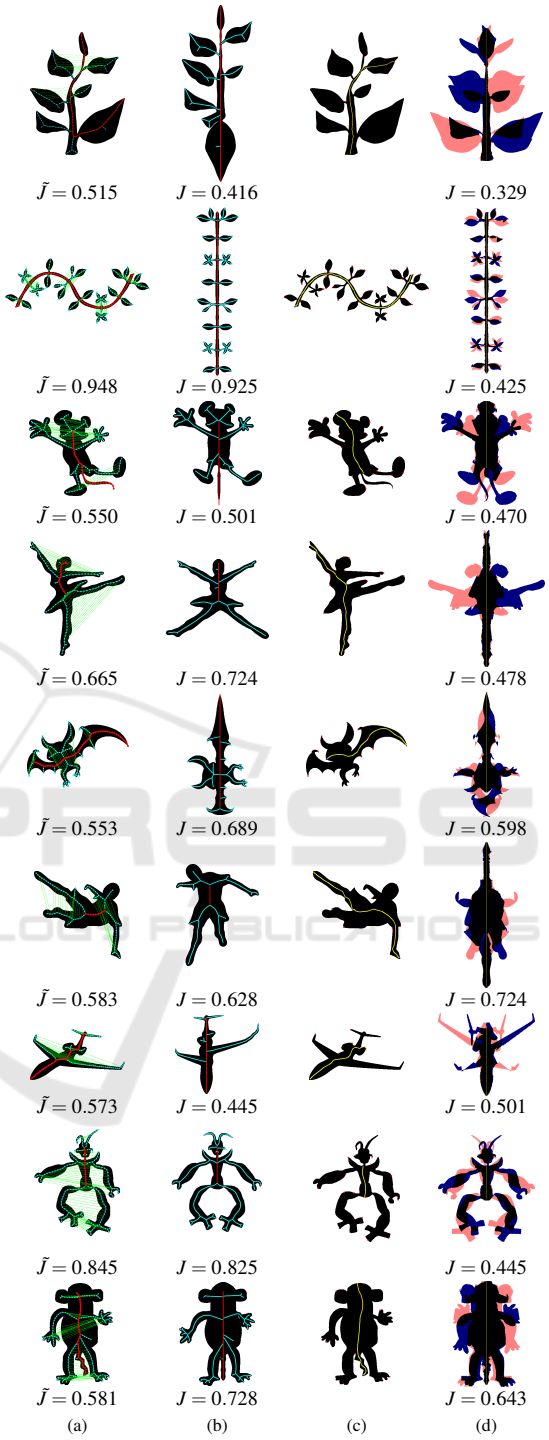

Figure 7: Restoration of symmetry in flexible shapes. Edge mapping by the proposed method (a) and the (Seredin et al., 2023) method (c). Shape straightening by the proposed method (b) and by the alternative method (d).

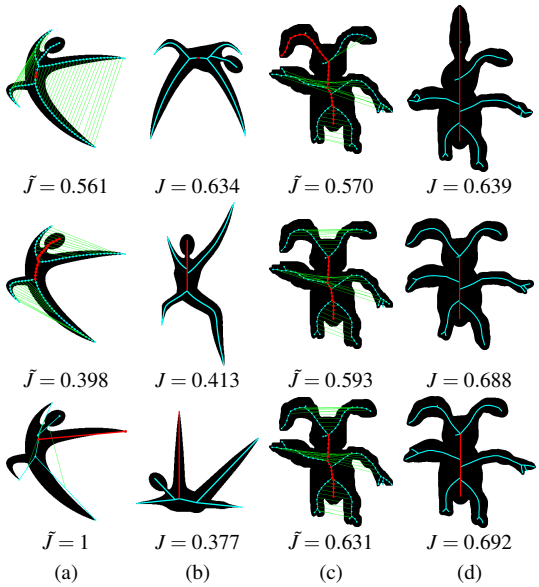

Figure 8: Symmetry Restoration Errors. A shape with unequal areas of its mapping (a) and straightening (b) regions. Results for various pruning parameters and the conversion from skeleton branches to edges: mapping (c) and straightening (d).

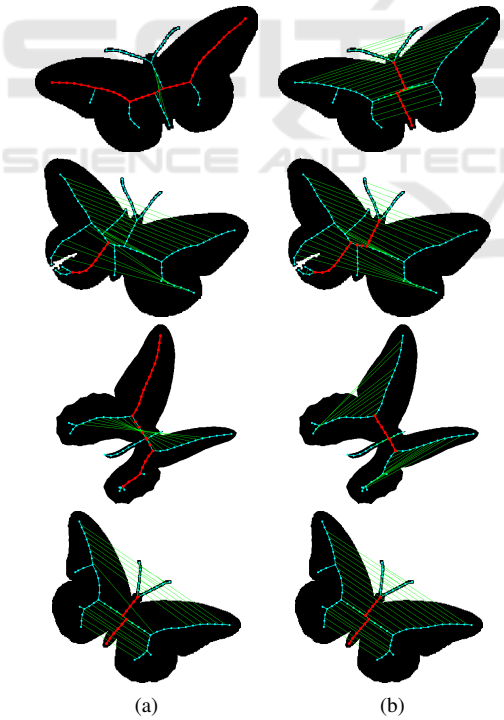

Figure 9: Finding the symmetry axis: (a) at the branch level, (b) at the edge level.

in 85 images when processing edges. Fig. 9 shows the difference in the results. Note that $\tilde{J}$ for the edge method is guaranteed to be no lower than that of the branch method since any correspondence between branches is representable as a correspondence between edges.

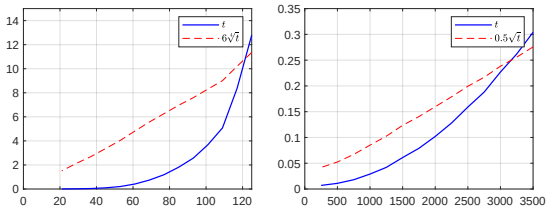

Figure 10: Time costs in seconds when processing (a) at the edge level, (b) at the branch level.

The general runtime vs. number of edges E curve is shown in Fig. 10. The experimental results agree well with the theory. The runtime increase pattern corresponds to $O(|E|^4)$ when comparing edges, $O(|E|^2)$ when comparing branches. When using the right exponents, the curves become linear. The average runtime of the alternative method is 0.313 seconds, which is roughly equivalent to running a method with 60 branches or 3500 edges.

9 CONCLUSION

We proposed a formal concept of symmetry in flexible planar shapes using their skeletons. The search for symmetry is reduced to finding the best mapping of the original and reflected skeletons of the shape. The optimized functional is defined in such a way as to resemble the Jaccard area index and can be used for its approximation. Since it consists of summands representing the comparisons of individual edges, the solution of the problem fits into the dynamic programming paradigm. We offered an analytical solution for distributing the shape area along the skeleton edges. The algorithm successfully restores the symmetry of complex flexible objects except for substantial differences in their areas (perspective distortions, for example). In the "fast" version, the pruning parameter has to be adjusted, while the "precise" version limits the number of edges. Future work involves generalizing the method to 3D shapes and, conversely, adaptation of already existing 3D methods to the planar case.

ACKNOWLEDGEMENTS

This work was supported by the Ministry of Science and Higher Education of the Russian Federation

within the framework of the state task FEWG-2024-0001.

REFERENCES

Bai, X. and Latecki, L. J. (2008). Path Similarity Skeleton Graph Matching. *IEEE Transactions on Pattern Analysis and Machine Intelligence*, 30(7):1282–1292.

Bai, X., Liu, W., and Tu, Z. (2009). Integrating contour and skeleton for shape classification. *2009 IEEE 12th International Conference on Computer Vision Workshops, ICCV Workshops*, pages 360–367.

Cicconet, M., Hildebrand, D. G. C., and Elliott, H. (2017). Finding Mirror Symmetry via Registration and Optimal Symmetric Pairwise Assignment of Curves. In *2017 IEEE International Conference on Computer Vision Workshops (ICCVW)*, pages 1749–1758.

Huang, H., Wu, S., Cohen-Or, D., Gong, M., Zhang, H., Li, G., and Chen, B. (2013). L1-medial skeleton of point cloud. *ACM Trans. Graph.*, 32(4):65:1–8.

Huang, J., Stoter, J., and Nan, L. (2023). Symmetrization of 2D Polygonal Shapes Using Mixed-Integer Programming. *Computer-Aided Design*, 163:103572.

Jiang, W., Xu, K., Cheng, Z.-Q., and Zhang, H. (2013). Skeleton-based intrinsic symmetry detection on point clouds. *Graphical Models*, 75(4):177–188.

Kushnir, O., Fedotova, S., Seredin, O., and Karkishchenko, A. (2017). Reflection Symmetry of Shapes Based on Skeleton Primitive Chains. In *Analysis of Images, Social Networks and Texts*, pages 293–304, Cham. Springer International Publishing.

Li, S., Liu, X., Cao, J., and Wang, S. (2019). Organic skeleton correspondence using part arrangements. *Applied Mathematics-A Journal of Chinese Universities*, 34:326–339.

Liu, J. and Liu, Y. (2011). Curved Reflection Symmetry Detection with Self-validation. In *Computer Vision – ACCV 2010*, pages 102–114, Berlin, Heidelberg. Springer Berlin Heidelberg.

Liu, T., Kim, V., and Funkhouser, T. (2012). Finding surface correspondences using symmetry axis curves. *Computer Graphics Forum*, 31(5):1607–1616.

Lomov, N. and Seredin, O. (2023). Dynamic Programming for Curved Reflection Symmetry Detection in Segmented Images. *The International Archives of the Photogrammetry, Remote Sensing and Spatial Information Sciences*, XLVIII-2/W3-2023:157–163.

Mestetskiy, L. and Semenov, A. (2008). Binary Image Skeleton – Continuous Approach. In *Proceedings of the Third International Conference on Computer Vision Theory and Applications - Volume 1: VISAPP, (VISIGRAPP 2008)*, pages 251–258. INSTICC, SciTePress.

Mestetskiy, L. M. and Koptelov, D. A. (2024). Constructing the Internal Voronoi Diagram of Polygonal Figure Using the Sweepline Method. *Program. Comput. Softw.*, 50(4):292–303.

Nagar, R. and Raman, S. (2018). Fast and Accurate Intrinsic Symmetry Detection. In *Computer Vision – ECCV 2018*, pages 433–450, Cham. Springer International Publishing.

Qian, Z., Zhuming, H., Hui, H., Kai, X., Hao, Z., Daniel, C.-O., and Baoquan, C. (2015). Skeleton-Intrinsic Symmetrization of Shapes. *Computer Graphics Forum*, 34(2):275–286.

Seredin, O., Liakhov, D., Lomov, N., Kushnir, O., and Kopylov, A. (2023). Greedy algorithm for fast finding curvilinear symmetry of binary raster images. In *Analysis of Images, Social Networks and Texts - 11th International Conference, AIST 2023, Yerevan, Armenia, September 28-30, 2023, Revised Selected Papers*, volume 14486 of *Lecture Notes in Computer Science*, pages 241–251. Springer.

Song, C., Pang, Z., Jing, X., and Xiao, C. (2018). Distance field guided L_1-median skeleton extraction. *The Visual Computer*, 34(2):243–255.

Wang, W., Ma, J., Xu, P., and Chu, Y. (2019). Intrinsic Symmetry Detection on 3D Models with Skeleton-guided Combination of Extrinsic Symmetries. *Computer Graphics Forum*, 38(7):617–628.

Xu, Z. and Zhang, Q. (2016). Symmetry-Aware Human Shape Correspondence Using Skeleton. In *MultiMedia Modeling*, pages 632–641, Cham. Springer International Publishing.

Yang, X., Adluru, N., Latecki, L. J., Bai, X., and Pizlo, Z. (2008). Symmetry of Shapes Via Self-similarity. In *Advances in Visual Computing*, pages 561–570, Berlin, Heidelberg. Springer Berlin Heidelberg.